

## Article

# Investigation on the Fragmentation and Outburst Mechanism of Coal Sample with Pore Gas Using CDEM

Qunlei Zhang <sup>1,2</sup>, Zhiming Wang <sup>2,3</sup>, Chun Feng <sup>4,5,\*</sup>, Xinguang Zhu <sup>4</sup> and Jun Zhou <sup>4</sup>

<sup>1</sup> School of Civil Engineering and Communication, North China University of Water Resources and Electric Power, Zhengzhou 450045, China

<sup>2</sup> School of Energy Science and Engineering, Henan Polytechnic University, Jiaozuo 454003, China

<sup>3</sup> Collaborative Innovation Center of Coal Work Safety, Jiaozuo 454000, China

<sup>4</sup> Institute of Mechanics, Chinese Academy of Sciences, Beijing 100190, China

<sup>5</sup> School of Engineering Science, University of Chinese Academy of Sciences (UCAS), Beijing 100190, China

\* Correspondence: fengchun@imech.ac.cn; Tel.: +86-13810614191

**Abstract:** In this paper, using the continuum-discontinuum element method (CDEM), the fragmentation and outburst process of coal specimen are simulated, and the main factors affecting coal breaking and outburst are explored. The results show that after the coal seam is uncovered, coal generates obvious failure and outburst trend. Near coal-free surface, the fracture coal blocks generate significant displacement, resulting in larger opening widths of coal cracks. Coal deep generates the cracks without an obvious opening width. The crack density of coal with pore gas is larger than those of coal without gas, and it is larger than those of coal without pores. However, in the early stage of coal failure, the obvious separation and outburst ranges of coal with gas are smaller than those of coal without gas, and are smaller than those of coal without pores. The numbers of fracture coal blocks show an increase with the growth of in situ stress, pore ratio and gas pressure. The effect of in situ stress on fracture coal block number (517–10,203) is larger than the effect (7589–15,170) of pore ratio and is larger than the effect (5803–6836) of gas pressure. The effect of in situ stress on a maximum size (0.0387–0.138 m) of fracture blocks is larger than the effect (0.0342–0.0733 m) of pore ratio and is larger than the effect (0.0454–0.0578 m) of gas pressure. The coal outburst velocity and range show an increase with the growth of gas pressure and in situ stress (3.77–5.65 m/s); however, the coal outburst shows a slow decrease with a growth of pore ratio. The effect of gas pressure on the coal outburst velocity (11.51–21.9 m/s) is larger than the effect (3.77–5.65 m/s) of in situ stress and is larger than the effect (4.52–5.23 m/s) of pore ratio. This investigation is beneficial to understand the mechanisms of coal–gas outburst in coal mining and roadway excavation.

**Keywords:** coal–gas outburst; in situ stresses; pore ratios; gas pressures; CDEM



**Citation:** Zhang, Q.; Wang, Z.; Feng, C.; Zhu, X.; Zhou, J. Investigation on the Fragmentation and Outburst Mechanism of Coal Sample with Pore Gas Using CDEM. *Minerals* **2023**, *13*, 351. <https://doi.org/10.3390/min13030351>

Academic Editor: Samintha Perera

Received: 23 December 2022

Revised: 18 February 2023

Accepted: 28 February 2023

Published: 1 March 2023



**Copyright:** © 2023 by the authors. Licensee MDPI, Basel, Switzerland. This article is an open access article distributed under the terms and conditions of the Creative Commons Attribution (CC BY) license (<https://creativecommons.org/licenses/by/4.0/>).

## 1. Introduction

Coal is a critical natural resource in the world, which provides large amounts of energy and raw materials for meeting industrial demands in China, America, India, Indonesia, etc. [1,2]. With mining depth becoming larger, the dynamic hazards induced by gas and mining disturbance are raised, especially coal and gas outburst [3]. The coal and gas outburst hazards always occur in mining during the operation of rock cross-cut coal uncovering. As of now, four coal and gas outburst accidents occurred in China in 2022 alone, resulting in five deaths and large economic losses. Therefore, it is very urgent to illuminate the happening mechanism of the coal and gas outburst during the rock cross-cut coal uncovering.

Gas, mainly composed of methane, is stored in coal seam with two typical statuses, which are adsorption and free status [4]. The coal-rock seam maintains balance without excavation and any other mining disturbances. However, with roadway excavation in coal seam or rock layer, the in situ stress is redistributed, causing the change of the stress

imposed on the mechanical unit of coal, which leads to the damage formation even if the whole crack is in the coal rock [5]. The gas pressure, in situ stress and the initial pores/fracture of the coal are the main factors influencing the damage and crack evolution. By CT scanning, Wu et al. [6] studied the coal damage and crack propagation with different gas pressures and found that the various trends of the stress-strain curve of coal samples under different gas pressures are similar. Whereas, with the increase in gas pressure, the 2D-fractal dimension value of the fracture net increases linearly. Li et al. [7] studied the influences of mining disturbance on the damage and permeability of coal samples and found that coal permeability decreases with the increase in loading cycle, while the damage in coal accumulates with the increase in loading cycle. Jiang et al. [8] analyzed the effects of pore and fracture structure on coal and gas outburst, proving that the fault in coal significantly influences the pore structure, which contributes to it being prone to coal and gas outburst. Besides, the responses of acoustic emission, deformation and electric potential power are usually used to predict the coal and gas outburst accident, which have been studied for a long time [9–11].

Considering the complexity of coal and gas outburst, the successive observations of the outburst process are difficult in engineering, and the limited test data in the outburst process of coal and gas can be obtained in the experiment [12,13]. With the development of computer technology, the numerical simulation has become an effective means to further and synthetically study the fragmentation and throwing mechanism of coal during coal and gas outburst process [14]. Wang et al. [15,16] established a numerical model considering the continuous damage with deformation, which could describe the damage evolution well and has been applied to study coal seam gas extraction. Qin et al. [17] Developed a coupled model of coal deformation and gas seepage for simulating the coal and gas outburst, proving that the gas pressure and unloading cross-section area are the two main factors influencing the stress redistribution and gas migration in seam. Cao et al. [18] adopted COMSOL software, which simulated the variations of stress, deformation and gas migration in coal, illuminating that the gas pressure gradient is necessary for the coal and gas outburst hazard. However, the microdamage mechanism of coal at the coal and gas outburst accident has not been studied well, thus hindering the development of the prevention method.

The above simulation research on coal–gas outburst are mainly by the finite element method. Although the permeation process of gas in coal mass can be accurately calculated, the fragmentation and movement of coal mass under the mining disturbance cannot be well characterized. Currently, a continuum-discontinuum element method (CDEM) combines the advantages of finite element method and discrete element method, which has gradually become an effective simulation method to study the failure and breaking mechanisms of coal and rock [19–26]. Based on CDEM, Feng et al. [19] studied the damage and fracture process of rock under the impact loading. Zhang et al. [20,21] investigated the top-coal caving in extra-thick coal seams and the automated top-coal drawing technique in extra-thick coal seams was optimized. Zhang et al. [22] simulated and analyzed the tensile fracture mechanisms of isotropic rock and anisotropy rock in Brazilian tests. However, based on CDEM, the research on the coal and gas outburst has not been reported in the literature.

In this paper, during the coal seam mining and roadway excavation process, the coal and gas outburst in deep rock cross-cut coal uncovering is simulated using the continuum-discontinuum element method (CDEM). Through the simulation analysis and comparison of the fragmentation and outburst characteristics of coal specimen under different working conditions, the main factors affecting coal breaking and outburst are explored. The failure models of coal mass are analyzed by the crack distribution of coal samples, while the range and degree of coal–gas outburst are analyzed by the outburst displacement and velocity of fracture coal blocks, and finally, the fracture degree of coal mass are analyzed by the characteristic count of fracture coal blocks.

## 2. Materials and Methods

### 2.1. The Continuum-Discontinuum Element Method

Based on the basic framework of the generalized Lagrange equation, a continuum-discontinuum element method (CDEM) is independently proposed by the Institute of Mechanics, Chinese Academy of Sciences [23]. The method integrates continuum numerical method with non-continuum numerical method, which realizes the unification of finite element, discrete element and meshless algorithm. In recent years, CDEM mechanical analysis software have been successfully applied in geotechnical engineering, mining and other fields [19–26].

CDEM adopts an incremental explicit algorithm to solve the dynamic problem, which mainly includes two parts: node force calculation and node motion calculation.

The calculation formula of node motion is:

$$\begin{cases} a = F/m & v = \sum_{t=0}^{T_{now}} a \Delta t \\ \Delta u = v \Delta t & u = \sum_{t=0}^{T_{now}} \Delta u \end{cases} \quad (1)$$

where  $v$  is node initial speed,  $a$  is node initial speed,  $\Delta u$  is node increment displacement,  $u$  is node displacement,  $m$  is node quality and  $\Delta t$  is the time step.

The calculation formula of node force is:

$$F = F^E + F^b + F^c + F^l + F^g \quad (2)$$

where  $F$  is resultant force for nodes,  $F^E$  is node external force,  $F^b$  is nodal force due to element deformation,  $F^c$  is the contact force on the node,  $F^l$  is the local damping force of node and  $F^g$  is the nodal force due to gas expansion.

For the gas element in coal pore, the deformation and stress of air element are expressed by the gas expansion equation:

$$p = p_0 \left( \frac{V_0}{V} \right)^\gamma \quad (3)$$

where  $p$  and  $p_0$  denote gas pressure in initial and current state,  $V$  and  $V_0$  mean the volume of element in initial and current state and  $\gamma$  represents adiabatic exponent (4/3 is adopted in this paper).

For the solid element of coal samples, the deformation and stress of block element are expressed by incremental method:

$$\begin{aligned} \Delta \xi_i &= B_i \cdot \Delta u \\ \Delta \sigma_i &= D \cdot \Delta \xi_i \\ \sigma_i^n &= \sigma_i^0 + \Delta \sigma_i \\ F_b &= \sum_{i=1}^N B_i^T \cdot \sigma_i^n \cdot \omega_i \cdot J_i \end{aligned} \quad (4)$$

where  $i$  is the element Gaussian point,  $\Delta \xi_i$  is the incremental strain vector,  $B_i$  is the strain matrix,  $\Delta u$  is the node incremental displacement vector,  $\Delta \sigma_i$  is the incremental stress vector,  $D$  is the element elastic matrix,  $\sigma_i^n$  is the total stress at the current step,  $\sigma_i^0$  is the total stress at the previous step,  $F_b$  is the node force vector,  $N$  is the number of Gaussian points,  $\omega_i$  is the integral coefficient and  $J_i$  is the Jacobian determinant value.

The interaction between these element interfaces can be transformed by the virtual spring forces. The forces at the contact interface of two blocks in the local coordinate can be expressed as:

$$\begin{aligned} F_n &= -K_n \times \Delta u_n \\ F_s &= -K_s \times \Delta u_s \end{aligned} \quad (5)$$

where  $F$ ,  $K$  and  $\Delta u$  are the incremental force, stiffness and relative displacement of the virtual spring, respectively, and  $n$  and  $s$  represent the normal and tangential directions, respectively.

In this paper, the maximum tensile stress criterion and Mohr–Coulomb with tension cut off criterion are used to characterize the damage fracture of interface element.

In calculation, the maximum tensile stress criterion is used to correct the normal stress of interface element:

$$\begin{aligned} & \text{If } F_n \geq \sigma \times A_c \\ & \text{Then } \sigma = 0; F_n = 0 \end{aligned} \tag{6}$$

where  $\sigma(t)$  is the tensile strength of interface virtual spring and  $A_c$  stands for the effective area of element interface.

In calculation, Mohr–Coulomb with tension cut off criterion is used to correct the tangential stress of interface element:

$$\begin{aligned} & \text{If } F_s \geq F_n \times \tan \phi + c \times A_c \\ & \text{Then } c = 0; F_s = F_n \times \tan \phi \end{aligned} \tag{7}$$

where  $\phi$  denotes the internal friction angle of interface element and  $c$  stands for the cohesion strength.

Based on the above equations, the coupling algorithm of coal and gas is achieved by the diagram of simulation procedure, as indicated in Figure 1:

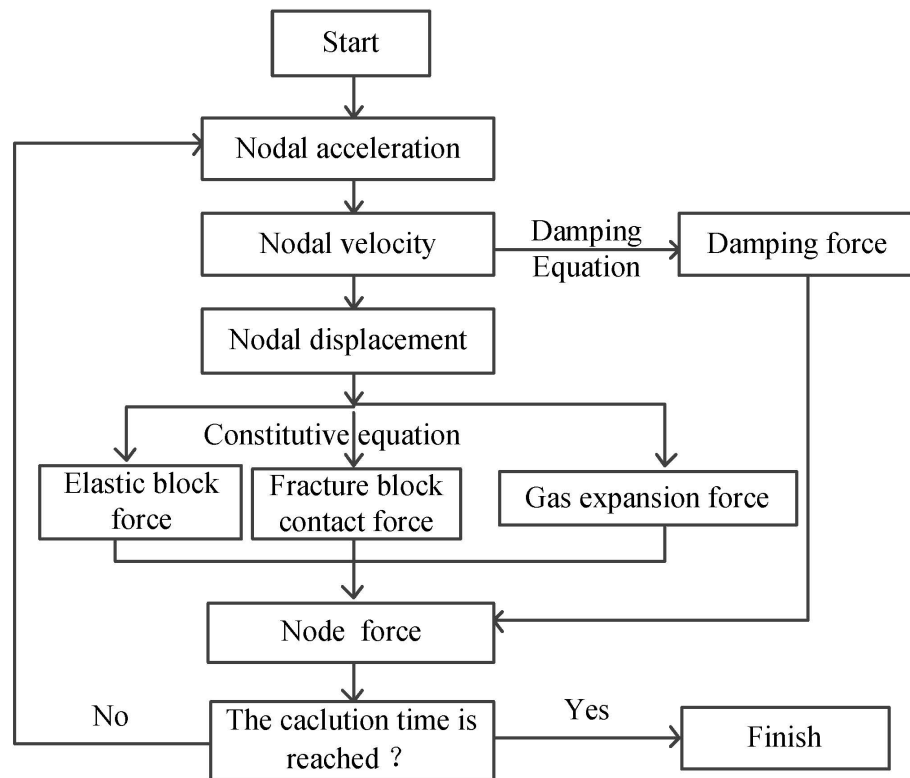


Figure 1. The simulation procedure diagram of coal and gas coupling.

For the verification of the simulation method, in reference [22], the foliation-affected fracturing of isotropic and anisotropy rock was simulated by CDEM and the results were compared with the experimental results, which indicates the applicability of numerical methods on the rock tensile failure. In reference [27], the deformation and fracture characteristics of coal gangue interbedded samples under loading and unloading conditions were investigated, which indicates the applicability of numerical methods on the rock compressive failure. In this paper, based on CDEM, the fragmentation and outburst mechanism of coal with pore gas are investigated.

2.2. Numerical Model, Parameter and Simulation Scheme

2.2.1. Numerical Model

To analyze the fracture and outburst mechanism of coal mass in mining and roadway excavation process, the models of coal samples without pores, with pores and with pore gas are generated, respectively, as shown in Figure 2. The sizes of numerical samples are 15 mm × 15mm, the mesh size is 1mm and about 60,000 triangular elements are generated. The pore ratio of the coal sample is the ratio of pore volume and coal volume, and the coal pore distributions are generated by the random generation algorithm in CDEM. The white part in Figure 2b is the pore distribution of the coal sample and the black part in Figure 2c presents the pore gas distribution of the coal sample. The boundary conditions of numerical models are consistent, and the vertical distributed stress are applied at the model top and bottom, which is used to generate the initial ground stress of coal seam before mining in simulation. The normal displacements are constrained around the model, which is used to characterize the initial state before coal mining. The boundary constraints on one side of the model are removed, which is used to characterize the coal seam is uncovered.

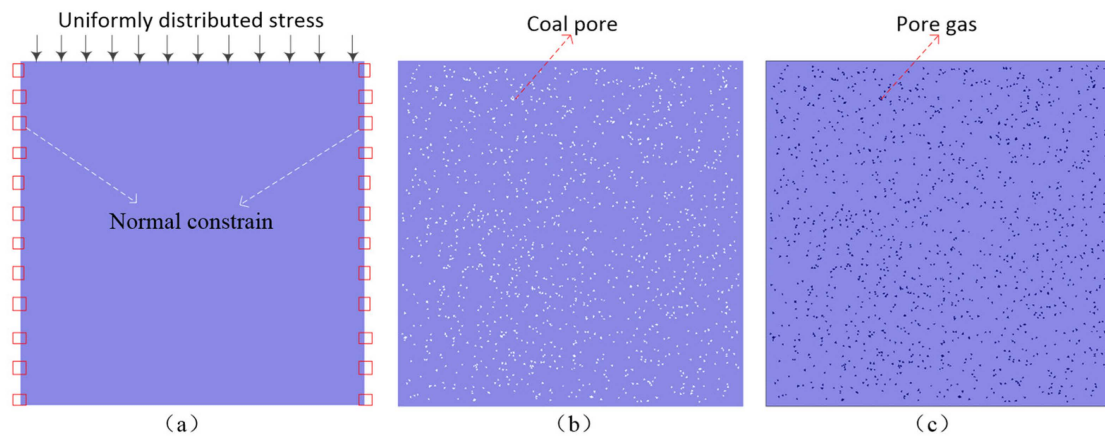


Figure 2. The coal models: (a) coal without pores; (b) coal with pores; and (c) coal with pore gas.

2.2.2. Material Properties

This study aims to analyze the fragmentation and outburst mechanism of coal with gas in mining and roadway excavation process. Under different simulation conditions, the physical and mechanical parameters of coal samples are shown in Table 1 [27,28], which is used to calculate the force-deformation and fracture by the Equations (4)–(7). The mechanical parameters of pore gas are shown in Table 2 [29], which is used to calculate the expansion and force of pore gas by the Equation (3), and the coupling effect of void gas and coal elements is realized by contact element by the Equation (5).

Table 1. The coal mechanical parameters.

Property	Density (kg/m <sup>3</sup> )	Elastic Modulus (GPa)	Poisson's ratio	Cohesion (MPa)	Tensile Strength (MPa)	Internal Friction Angle (°)
Coal	1300	2.69	0.34	2.5	1	35

Table 2. Gas expansion mechanical parameters.

Property	Density (g/L)	Initial Pressure (MPa)	Adiabatic Exponent
Gas	0.717	0–2	4/3



### 2.2.3. Simulation and Analysis Schemes

During the coal seam mining and roadway excavation process, the right constraint of coal model is deleted, which indicates the coal seam is uncovered, then the coal and gas outburst in deep rock cross-cut coal uncovering is simulated. Through the simulation analysis and comparison of coal specimen failure under different working conditions, the main factors affecting coal breaking and outburst are explored. Concretely, the in situ stresses (5 MPa, 7.5 MPa, 10 MPa and 12.5 MPa) loaded on coal samples are used to investigate the effects of coal depths (200 m, 300 m, 300 m and 400 m) on coal failure; the pore ratios (0.01, 0.025, 0.05 and 0.075) of coal samples are used to investigate the effects of pore ratio on coal failure, and the vertical stress of the coal sample is 10 MPa; the initial gas pressures (0.5 MPa, 1 MPa, 1.5 MPa and 2 MPa) in coal pores are used to investigate the effects of initial gas pressure on coal and gas outburst, where the vertical stress of the coal sample is 10 MPa and the pore ratio of the coal sample is 0.025. The crack distribution of numerical samples is used to analyze the failure model of coal mass, the displacement and velocity of fracture coal blocks are used to analyze the failure range and degree of coal mass, and the characteristic count of fracture coal blocks is used to analyze the fracture degree of coal mass.

## 3. Results

### 3.1. Effect of Different Vertical Stress on Coal Failure

To study the effects of in situ stress on coal mass failure, the failure process of coal samples loaded on different vertical stresses (5 MPa, 7.5 MPa, 10 MPa and 12.5 MPa) are simulated, which characterizes the in situ stress of coal depths (200 m, 300 m, 300 m and 400 m). The crack distribution, displacement contour and velocity contour of numerical samples are shown in Figure 3.

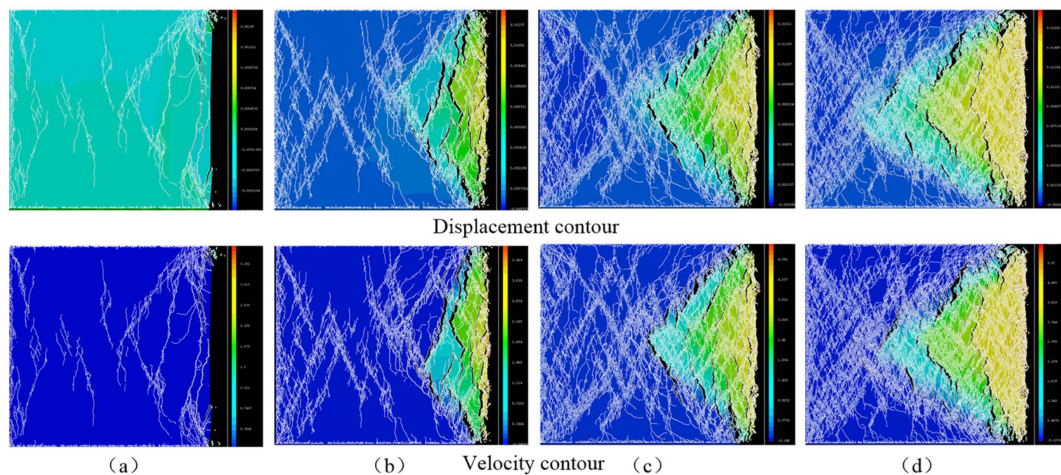


**Figure 3.** The crack distribution, displacement contour and velocity contour of numerical samples under different in situ stresses: (a) vertical stresses 5 MPa; (b) vertical stresses 7.5 MPa; (c) vertical stresses 10 MPa; and (d) vertical stresses 12.5 MPa.

From Figure 3, as the coal seam is uncovered, the coal sample generates obvious failure, and the fracture coal blocks show an obvious outburst trend toward the direction of free surface. On the side of free surface, the fracture coal blocks generate significantly horizontal displacement, and there exists larger opening widths of coal cracks. On the deep side of coal, the coal sample also generated the fracture phenomenon; however, there are no obvious opening widths of coal cracks. Under different in situ stress conditions, the failure degree of coal samples shows an obvious increasing trend with an increase in in situ stress. Concretely, as shown in Figure 3a, under the vertical loading stress of 5 MPa, some major cracks generate on the coal sample, resulting in a major crack with a larger opening

width near the free surface and the fracture coal blocks with smaller size and number are thrown out at a certain speed. As shown in Figure 3b, under the vertical loading stress of 7.5 MPa, the number of coal cracks are obviously larger than that of 5 MPa in situ stress, where multiple main cracks of the coal sample have obvious opening widths near the free surface. However, the range of the coal sample generating obvious displacement are larger than the range of the coal sample generating obvious velocity. As shown in Figure 3c, under the vertical loading stress of 10 MPa, more cracks generate on the coal sample and the range of the coal sample generating obvious displacement and velocity expands to the sample middle. As shown in Figure 3d, under the vertical loading stress of 12.5 MPa, the density and number of coal cracks continuously increase and the range of the coal sample generating obvious displacement and velocity expands to the coal deep.

To quantitatively analyze the variation law of coal failure under different in situ stresses, the maximum displacement and velocity statistics of fracture coal blocks are shown in Figure 4.

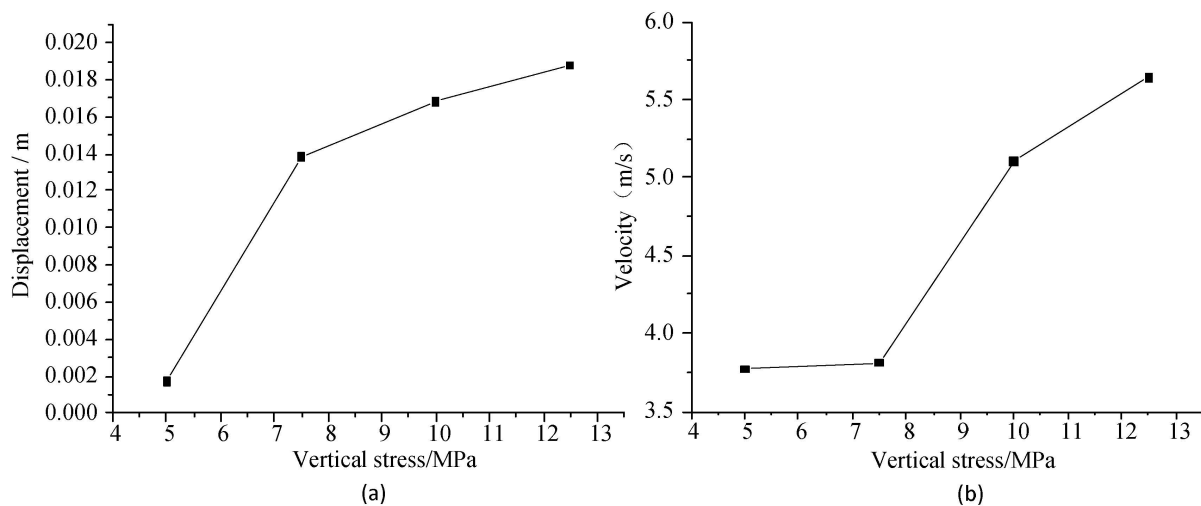


**Figure 4.** The maximum displacement and velocity statistics of the fracture block of the coal sample under different in situ stresses: (a) maximum displacement comparison of fracture coal blocks; (b) maximum velocity comparison of fracture coal blocks.

From Figure 4a, as the coal seam is uncovered, the outburst range of fracture coal blocks shows a nonlinear growth trend with an increase in vertical stress loaded on coal samples. Concretely, the outburst range of fracture coal blocks is 0.0017 m as the vertical loading stress is 5 MPa, the outburst range of fracture coal blocks is 0.0138 m as the vertical loading stress is 7.5 MPa, the outburst range of fracture coal blocks is 0.0168 m as the vertical loading stress is 10 MPa, and the outburst range of fracture coal blocks is 0.0188 m as the vertical loading stress is 12.5 MPa. From Figure 4b, after the right displacement constraint of the coal sample model is deleted, the outburst velocity of fracture coal blocks also shows a growth trend with an increase in in situ stress. Concretely, the outburst velocity of fracture coal blocks is 3.77 m/s as the in situ stress is 5 MPa, the outburst velocity of fracture coal blocks is 3.81 m/s as the in situ stress is 7.5 MPa, which is close to the outburst velocity of fracture coal blocks as the in situ stress is 5 MPa; however, the outburst velocity of fracture coal blocks rapidly increases to 5.11 m/s as the in situ stress is 10 MPa, and the outburst velocity of fracture coal blocks increases to 5.65 m/s as the vertical stress is 12.5 MPa.

To furtherly analyze the variation law of coal fragmentation, as the coal seam is uncovered, the characteristic block count of fracture coal under different in situ stresses are shown in Figure 5.

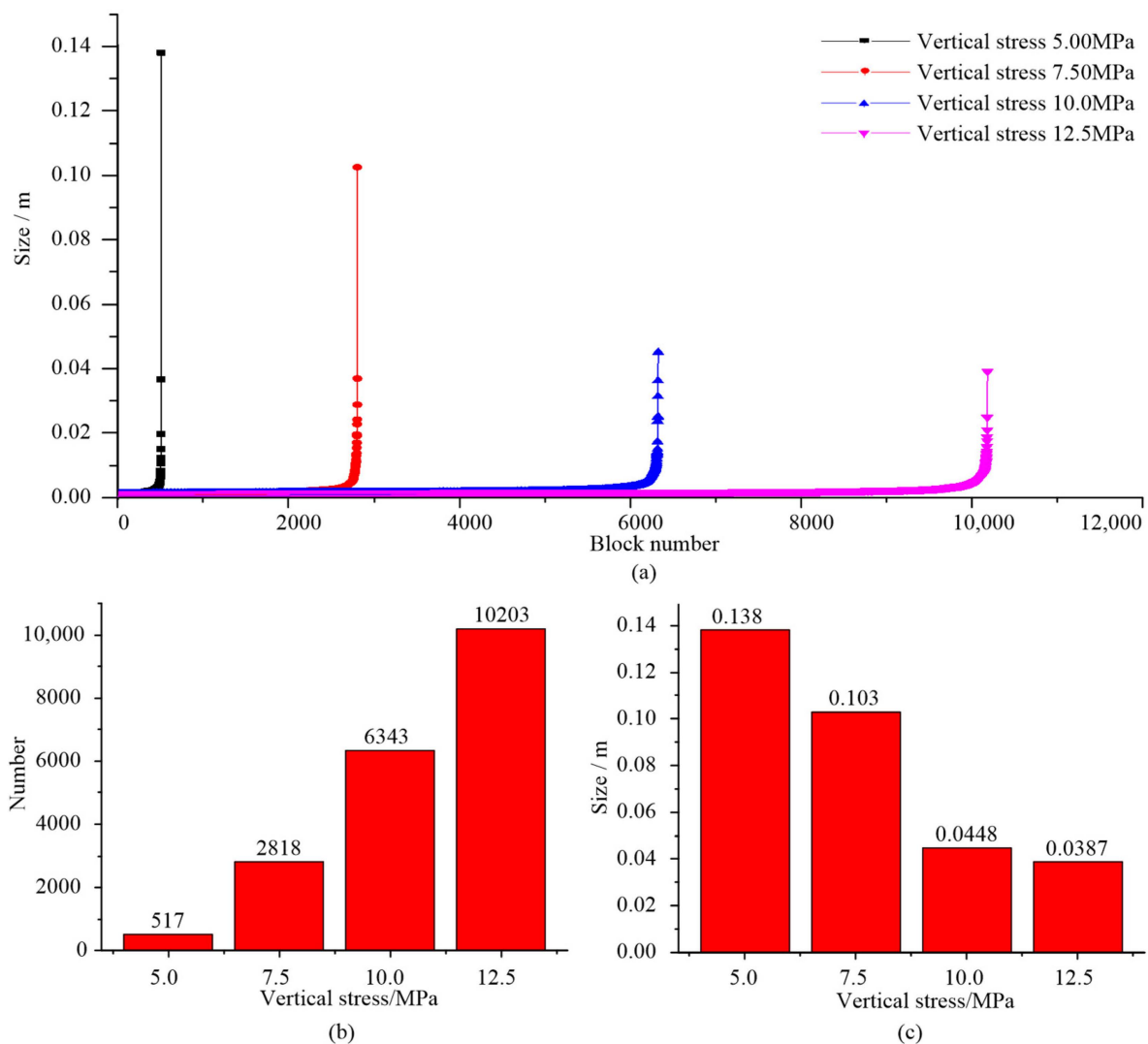


**Figure 5.** The maximum number and size statistics of the fracture block of coal samples under different in situ stresses: (a) characteristic size curves of fracture rock block; (b) fracture block number comparison; and (c) maximum block size comparison.

From Figure 5a, with an increase in in situ stress loaded on coal samples, the failure degree of coal samples shows an obvious growth trend and the number of fracture coal blocks rapidly increases; however, the maximum characteristic size of fracture coal blocks obviously decreases. Concretely, from Figure 5b, the block number of fracture coal is 517 as the vertical loading stress is 5 MPa, the fracture block number of the coal sample is 2818 as the vertical loading stress is 7.5 MPa, the fracture coal block number is 6343 as the vertical loading stress is 10 MPa, and the fracture block number is 10,203 as the vertical loading stress is 12.5 MPa. From Figure 5c, the maximum characteristic size of fracture coal blocks is 0.138 m as the vertical loading stress is 5 MPa, the maximum characteristic size of fracture coal blocks is 0.103 m as the vertical loading stress is 7.5 MPa, the maximum block size of fracture coal blocks is 0.0448 m as the vertical loading stress is 10 MPa, and the maximum characteristic size is 0.0387 m as the vertical loading stress is 12.5 MPa.

### 3.2. Effect of Different Pore Ratios on Coal Failure

To study the effects of pore ratios on coal mass failure, the failure process of coal samples with different pore ratios (0.01, 0.025, 0.05 and 0.075) are simulated, and the vertical stress of the coal sample is 10 MPa. The crack distribution, displacement contour and velocity contour of numerical samples with different pore ratios are shown in Figure 6.



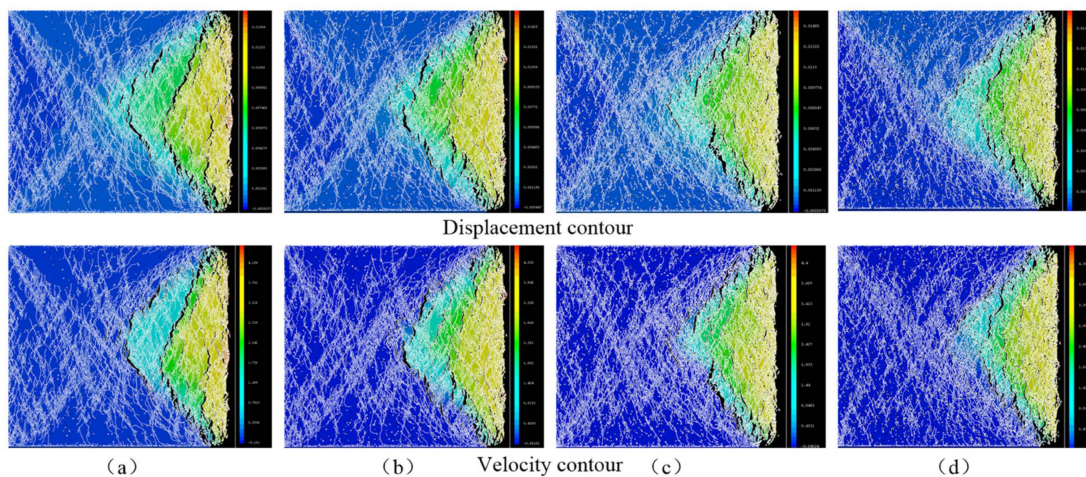


**Figure 6.** The crack distribution, displacement and velocity contour of numerical samples: (a) 0.01 of pore ratio; (b) 0.025 of pore ratio; (c) 0.05 of pore ratio; and (d) 0.075 of pore ratio.

From Figure 6, as the coal seam is uncovered, the coal sample generates a large number of cracks, and the fracture coal blocks show an obvious outburst trend toward the free-surface side of the coal sample, where there exists obvious opening widths of coal cracks on the free-surface side of the coal sample; however, there exists no obvious opening width of coal cracks on the coal deep. The ranges of coal samples generating obvious displacement are close to the ranges of coal samples generating obviously horizontal velocity. For different coal pore ratios, the density and number of coal cracks show an increasing trend with an increase in coal pore ratio; however, the ranges of coal samples generating obvious displacement and velocity show a decreasing trend with an increase in coal pore ratio.

To quantitatively analyze the variation law of coal fracture under different pore ratios, the maximum displacement and velocity statistics of fracture coal blocks are shown in Figure 7.

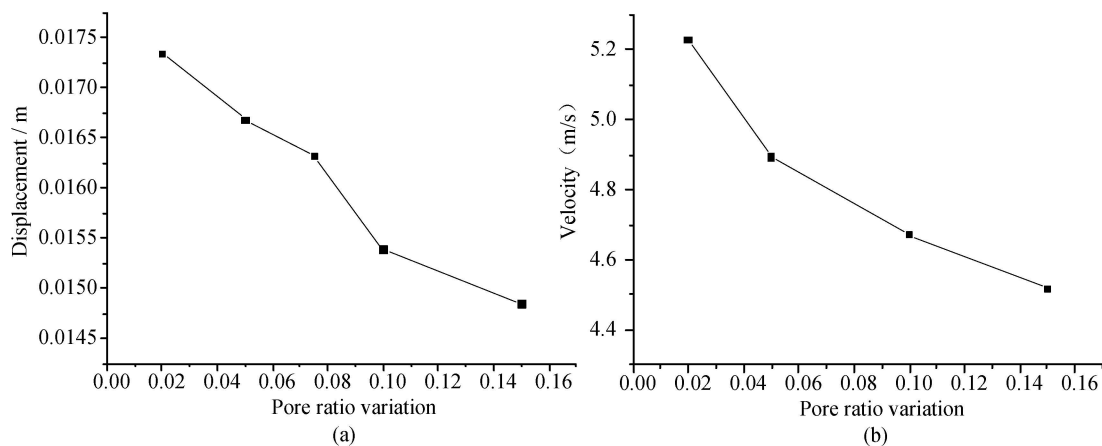


**Figure 7.** The maximum displacement and velocity statistics of fracture block of coal samples with different pore ratios: (a) maximum displacement comparison of fracture coal blocks; (b) maximum velocity comparison of fracture coal blocks.

From Figure 7a, as the coal seam is uncovered, the maximum outburst range of fracture coal blocks shows a nonlinear decreasing trend with an increase in coal pore ratio. Concretely, the outburst range of fracture coal blocks is 0.01734 m as the coal pore ratio is 0.02, the outburst range of fracture coal blocks is 0.01668 m as the coal pore ratio is 0.05, the outburst range of fracture coal blocks is 0.01632 m as the coal pore ratio is 0.075, the

outburst range of fracture coal blocks is 0.01538 m as the coal pore ratio is 0.1, and the outburst range of fracture coal blocks is 0.01484 m as the coal pore ratio is 0.15. From Figure 7b, after the coal seam is uncovered, the maximum velocity of fracture coal blocks also shows a decreasing trend with an increase in pore ratio. Concretely, the maximum outburst velocity of fracture coal blocks is 5.23 m/s as the pore ratio is 0.02, the maximum velocity of fracture coal blocks is 4.89 m/s as the pore ratio is 0.05, the outburst velocity of fracture coal blocks is 4.67 m/s as the pore ratio is 0.1, and the maximum velocity of fracture coal blocks is 4.52 m/s as the pore ratio is 0.15.

To furtherly analyze the variation law of coal fracture, the characteristic block count of fracture coal samples with different pore ratios are shown in Figure 8.

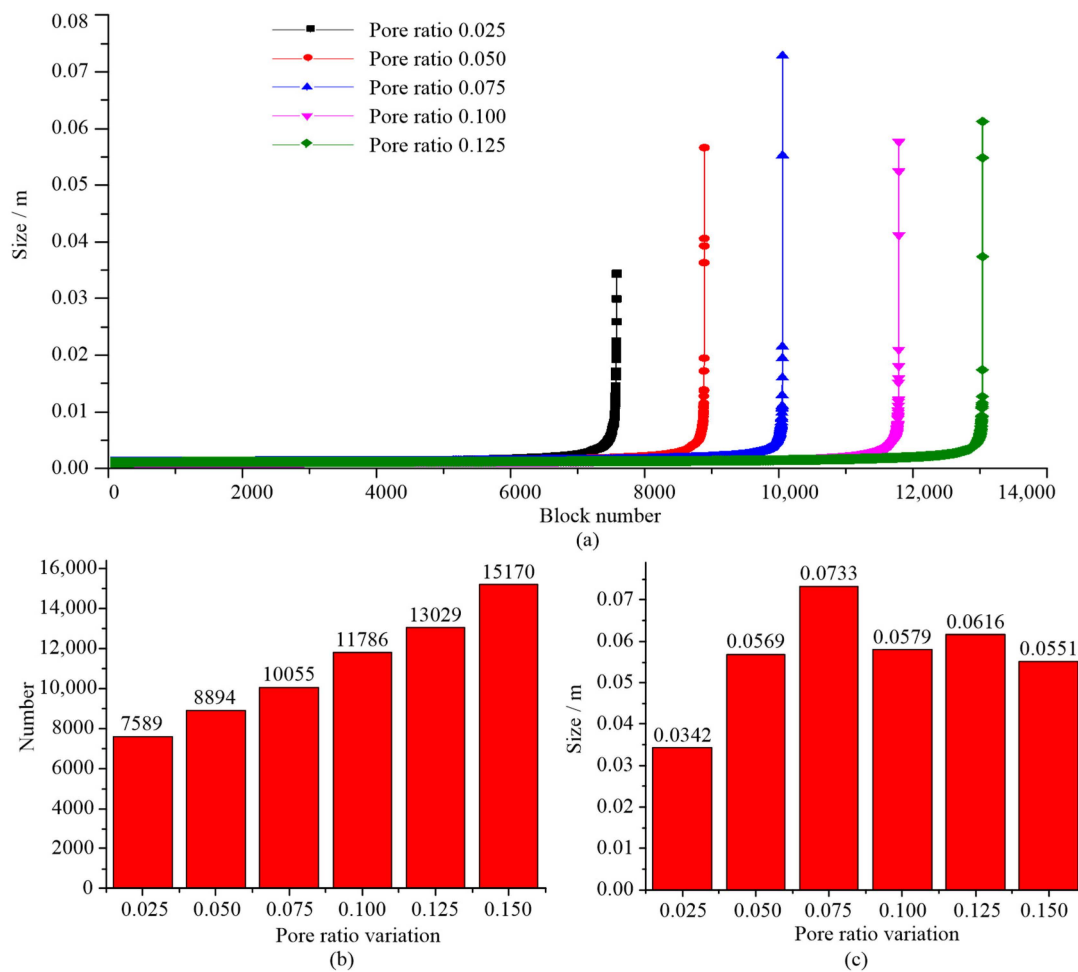


**Figure 8.** The maximum number and size statistics of the fracture block of coal samples with different pore ratios: (a) characteristic size curves of fracture rock block; (b) fracture block number comparison; and (c) maximum block size comparison.

From Figure 8a, with an increase in the pore ratio of coal samples, the failure degree of coal samples entirely shows an obvious growth trend and the number of fracture coal blocks rapidly increases. However, with an increase in the pore ratio of coal samples, the maximum characteristic size of fracture coal blocks firstly rapidly increases, then decreases, and finally, remains stable. Concretely, from Figure 8b, the block number of fracture coal slowly increases from 7589 to 10,055 as the coal pore ratio increases from 0.025 to 0.075; however, the block number of fracture coal increases from 10,055 to 15,710 with a larger change rate as the coal pore ratio increases from 0.075 to 0.15. From Figure 8c, the maximum characteristic size of fracture coal blocks rapidly increases from 0.0342 to 0.0733 m as the coal pore ratio increases from 0.025 to 0.075; however, the maximum characteristic size of

coal blocks decreases to 0.058 as the coal pore ratio increases from 0.1, and then remains relatively stable with the increase in coal pore ratio.

### 3.3. Effect of Different Pore Ratios on Coal Failure

To study the effects of pore gas pressure on coal mass failure, the failure process of coal samples with different gas pressures (0.01, 0.025, 0.05 and 0.075) are simulated in this section, where the vertical stress of the coal sample is 10 MPa and the pore ratio of the coal sample is 0.025. The crack distribution, displacement contour and velocity contour of numerical samples with different pore gas pressures are shown in Figure 9.

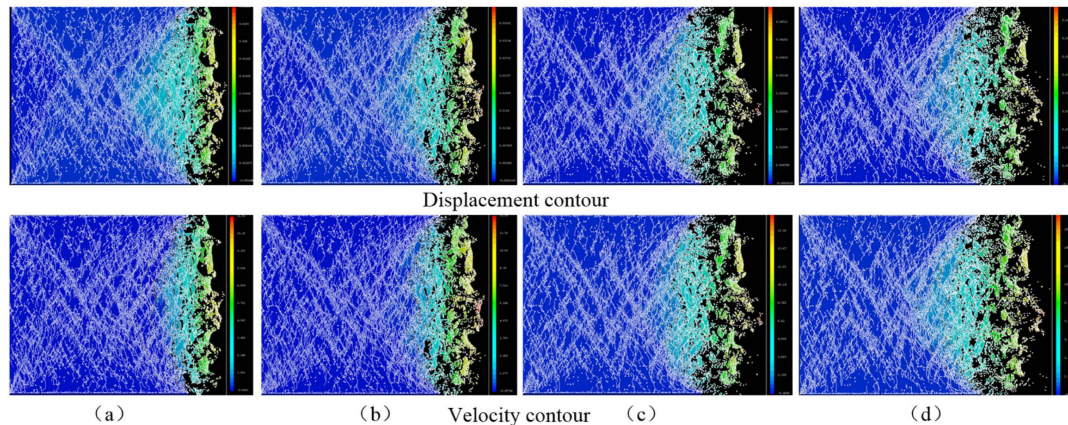


**Figure 9.** The crack distribution, displacement contour and velocity contour of numerical samples with different pore gas pressures: (a) 0.5 MPa gas pressure; (b) 1 MPa gas pressure; (c) 1.5 MPa gas pressure; and (d) 2 MPa gas pressure.

From Figure 9, as the coal seam is uncovered, more density and number of cracks generate on coal samples, and the fracture coal blocks are obviously thrown toward the free-surface direction; however, there exists no obvious opening width of coal cracks on the coal deep. For different pore gas pressures of coal samples, the crack density and number on coal deep show a decreasing trend with an increase in gas pressure; however, the outburst range of fracture coal blocks on the free-surface side show an obviously increasing trend with an increase in gas pressure. More concretely, as shown in Figure 9a,b, under the gas pressures of 0.5 MPa and 1 MPa, the ranges of coal samples generating obvious displacement are larger than the ranges of coal samples generating obvious velocity. As shown in Figure 9c,d, the ranges of coal samples generating obvious displacement are close to the ranges of coal sample generating obvious velocity.

To quantitatively analyze the variation law of coal fracture under different pore gas pressures, the maximum displacement and velocity statistics of fracture coal blocks are shown in Figure 10.

From Figure 10a, as the coal seam is uncovered, the outburst range of fracture coal blocks slowly grows from 0.03261 m to 0.03931 m as the gas pressure increases from 0.5 MPa to 1 MPa; however, the outburst range of fracture coal blocks rapidly grows from 0.03931 m to 0.06647 m as the gas pressure increases from 1 MPa to 2.25 MPa. From Figure 9b, as the coal seam is uncovered, the maximum velocity of fracture coal blocks slowly grows from 11.51 m/s to 12.58 m/s as the gas pressure increases from 0.5 MPa to 1 MPa; however, the maximum velocity of fracture coal blocks rapidly grows from 12.58 m/s to 21.9 m/s as the gas pressure increases from 1 MPa to 2.25 MPa.

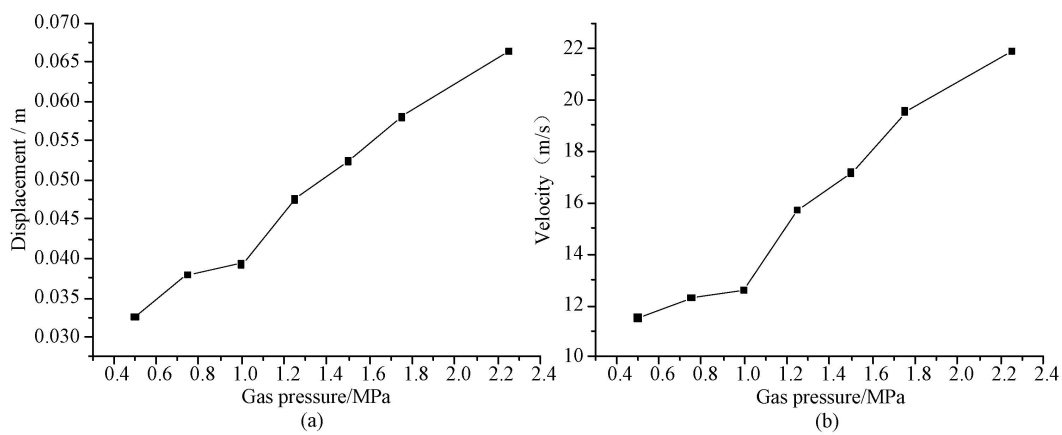


**Figure 10.** The maximum displacement and velocity statistics of the fracture block of coal samples with different pore gas pressures: (a) maximum displacement comparison of fracture coal blocks and (b) maximum velocity comparison of fracture coal blocks.

To further and quantitatively analyze the variation law of coal fracture, the characteristic block count of fracture coal under different gas pressures are shown in Figure 11.

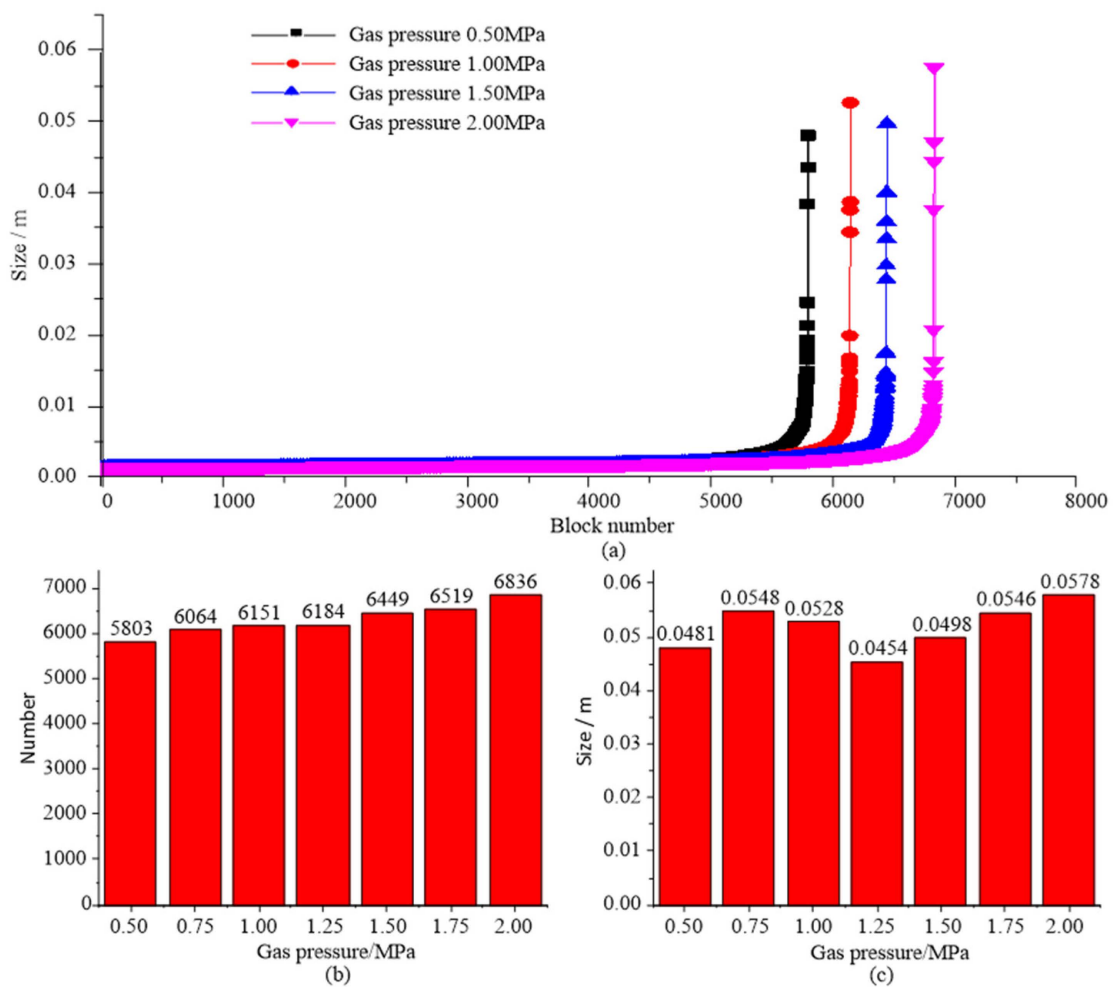


**Figure 11.** The maximum number and size statistics of the fracture block of coal samples with different pore gas pressures: (a) characteristic size curves of fracture rock block; (b) fracture block number comparison; and (c) maximum block size comparison.



From Figure 11a, with an increase in the gas pressure of coal pore, the failure degree of coal samples entirely shows an obvious growth trend and the number of fracture coal blocks rapidly increases. However, with an increase in gas pressure, the maximum characteristic size of fracture coal blocks shows an irregular change. Concretely, from Figure 11b, the block number of fracture coal slowly increases from 5803 to 6836 as the gas pressure of coal pore increases from 0.5 MPa to 2 MPa. From Figure 11c, the maximum characteristic size of fracture coal blocks ultimately remains about 0.05 m as the gas pressure of coal pore increases from 0.5 MPa to 2 MPa.

#### 4. Discussion

To comprehensively analyze the effects of different simulation conditions on coal mass failure, the failure processes of coal samples under different in situ stresses, pore ratios and gas pressures are compared. The crack distribution, displacement and velocity contour of numerical samples under different simulation conditions are shown in Figure 12.

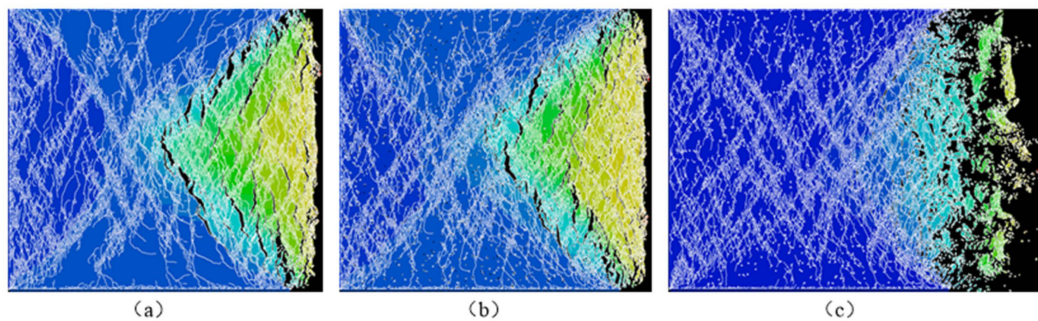


**Figure 12.** The failure result comparison of coal samples under different simulation conditions: (a) coal without pores; (b) coal with pores; and (c) coal with pore gas.

From Figure 12, as the in situ stress of the coal sample is 10 MPa, the pore ratio of the coal sample is 0.025, and the gas pressure of coal pore is 1 MPa, where the crack distribution, fragmentation and migration characteristic of coal samples are significantly different under different conditions. Concretely, under the vertical loading stress of 10 MPa shown in Figure 11a, a large number of cracks generate on the coal sample without pores, and multiple cracks have obvious opening widths near the free-surface side of the coal sample. There is also obvious migration displacement and outburst velocity of fracture coal blocks near the free surface. As shown in Figure 11b, for the coal sample with pores, the density and number of coal cracks are larger than those of the coal sample without pores; however, the ranges of the coal sample generating obvious displacement and outburst velocity are smaller than those of the coal sample without pores. As shown in Figure 11c, more density and number of cracks generate on the coal sample with pore gas and the obvious outburst range of fracture coal blocks on the free-surface side are significantly larger than those of the coal sample without gas. However, the ranges of generating obvious displacement on coal deep are significantly smaller than those of the coal sample without gas. This may be because, in the early stage of coal and gas outburst (0–3.3 ms), as the pore gas is pushing the broken coal block outward, it also has a reverse pushing effect on deep coal; therefore, there is a certain lag on the separation and outburst of deep coal.

To comprehensively analyze the variation law of coal fracture, the maximum displacement, maximum velocity, fracture coal block number and characteristic block of coal samples under different simulation conditions are shown in Figure 13.

From Figure 13a, the fracture block numbers of coal samples show an increasing trend with the growth of in situ stress, pore ratio and pore gas pressure. Concretely, the fracture block number of the coal sample with pores is obviously larger than that of the coal sample without pores, and the fracture block number of the coal sample with pore gas is obviously smaller than that of the coal sample without pore gas. Under different pore ratios and in



situ stresses, the block number variations of fracture coal are obvious; however, the block number variation of fracture coal is smaller with a variation of gas pressure. Generally, the effect of in situ stress on fracture coal block number is larger than the effect of pore ratio, which is larger than the effect of pore gas pressure.

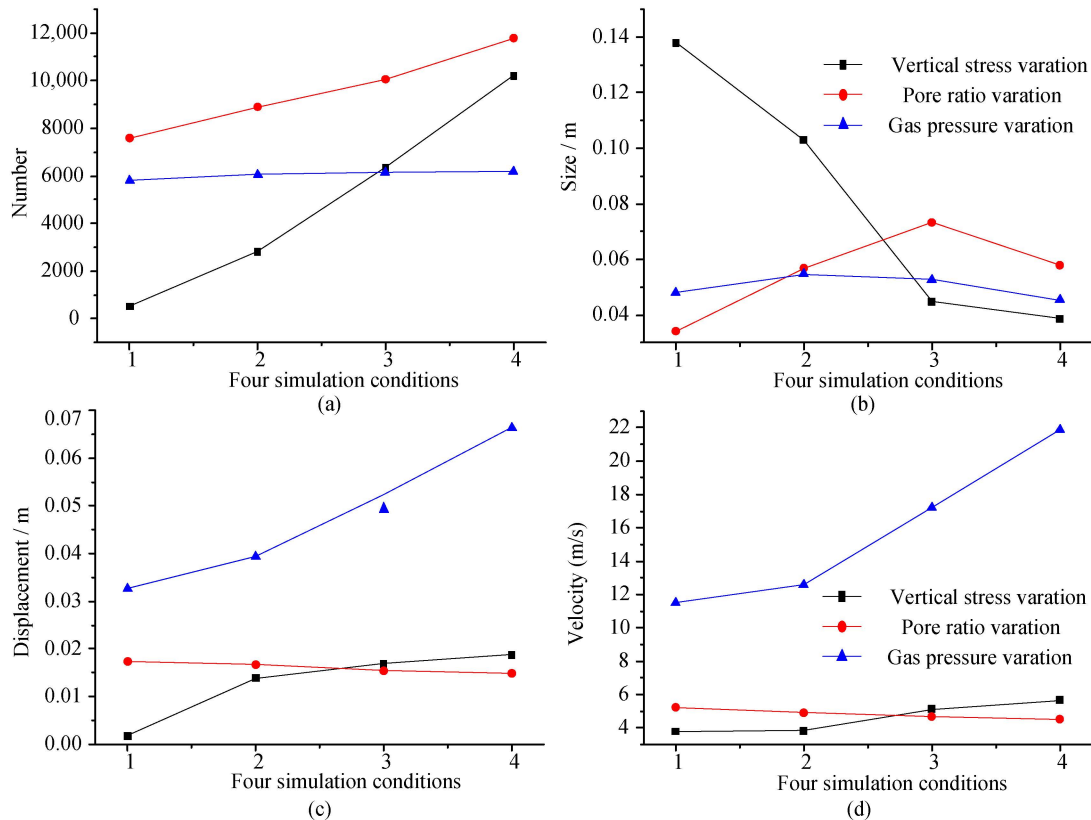


**Figure 13.** Comparison of the statistical results of coal failure under different simulation conditions: (a) fracture coal block number comparison; (b) maximum coal block size comparison; (c) maximum displacement comparison of fracture coal blocks; and (d) maximum velocity comparison of fracture coal blocks.

From Figure 13b, the maximum characteristic size of fracture coal blocks shows a rapidly decreasing trend with the growth of in situ stress, while the maximum size of fracture coal blocks first slowly increases and then decreases with the growth of coal pore ratio, and the maximum block size shows a smaller change with the variation of pore gas pressure. Generally, the effect of in situ stress on the maximum size of fracture coal blocks is larger than the effect of coal pore ratio, which is larger than the effect of pore gas pressure.

From Figure 13c, the effective outburst range of fracture coal blocks shows a rapidly increasing trend with the growth of pore gas pressure, while the outburst range of fracture coal blocks shows an increasing trend with the growth of in situ stress; however, the outburst range of fracture coal blocks shows a slowly decreasing trend with the growth of pore ratio. Generally, the effect of pore gas pressure on the outburst range of fracture coal blocks is larger than the effect of in situ stress, which is larger than the effect of pore ratio.

From Figure 13d, the maximum outburst velocity of fracture coal blocks shows a rapidly increasing trend with the growth of pore gas pressure, while the maximum velocity of fracture coal blocks shows a slowly increasing trend with the growth of in situ stress; however, the maximum velocity of fracture coal blocks shows a slowly decreasing trend with the growth of pore ratio. Generally, the effect of pore gas pressure on the maximum velocity of fracture coal blocks is obviously larger than the effect of in situ stress and the effect of in situ stress is slightly larger than effect of pore ratio.

## 5. Conclusions

In this paper, the coal specimen failures under different in situ stresses, pore ratios and pore gas pressures are simulated based on the continuum-discontinuum element method (CDEM). The main factors affecting coal breaking and outburst are explored through the analysis and comparison of the failure models, the range and degree of coal–gas outburst, and the fragmentation characteristic of fracture coal blocks. Some conclusions can be drawn:

(1) As the coal seam is uncovered, the coal sample generates obvious failure, and the fracture coal blocks show an outburst trend. Near coal-free surface, the fracture coal blocks generate significant outburst displacement and velocity, and there exists larger opening widths of coal cracks. On the coal deep, coal samples also generate the fracture phenomenon; however, there exists no obvious opening width of coal cracks.

(2) For the coal sample with pores, the density and number of coal cracks are larger than those of the coal sample without pores; however, the ranges of the coal sample generating obvious separation and outburst trend are smaller than those of the coal sample without pores. For the coal sample with pore gas, more density and number of cracks are generated, and the ranges of the coal sample generating obvious displacement and outburst trend are significantly smaller than those of the coal sample without gas in the early stage of coal–gas outburst; however, the obvious outburst range and velocity of fracture coal blocks are significantly larger than those of the coal sample without gas.

(3) The fracture block numbers of coal samples show an increasing trend with the growth of in situ stress, pore ratio and pore gas pressure. The effect of in situ stress on fracture coal block number is larger than effect of pore ratio, which is larger than the effect of pore gas pressure. The maximum characteristic size of fracture coal blocks shows a rapidly decreasing trend with the growth of in situ stress, while the maximum block size first slowly increases and then decreases with the growth of coal pore ratio, and the maximum size shows a smaller change with the variation of pore gas pressure. Generally, the effect of in situ stress on the maximum size of fracture coal blocks is larger than the effect of coal pore ratio, which is larger than the effect of pore gas pressure.

(4) The outburst velocity and outburst range of fracture coal blocks shows a rapidly increasing trend with the growth of pore gas pressure, while the outburst velocity and outburst range show an increasing trend with the growth of in situ stress; however, the outburst velocity and outburst range shows a slowly decreasing trend with the growth of pore ratio. Generally, the effects of pore gas pressure on the outburst velocity and outburst range of fracture coal blocks are larger than the effects of in situ stress, which are larger than the effects of pore ratio.

**Author Contributions:** Data curation, writing—original draft, formal analysis and writing—review and editing, Q.Z., Z.W. and C.F. Software and Methodology, X.Z. and J.Z. Writing—review and funding acquisition, Z.W. and C.F. All authors have read and agreed to the published version of the manuscript.

**Funding:** This research was supported by the National Key Research and Development Program of China, grant number 2018YFC1505504; Science and Technology Project of Henan province, grant number 222102320295; Fundamental Research Funds for the Universities of Henan Province, grant number NSFRF220441; and Key Scientific Research Projects of Colleges and Universities in Henan Province, grant number 23A440003.

**Data Availability Statement:** All the relevant data and models used in the study have been provided in the form of figures and tables in the published article.

**Conflicts of Interest:** The authors declare no conflict of interest to this work.

## References

1. Balat, M. Coal in the global energy scene. *Energy Source Part B Econ. Plan. Policy* **2010**, *5*, 50–62. [[CrossRef](#)]
2. Lahiri, K. The diverse worlds of coal in India: Energising the nation, energising livelihoods. *Energy Policy* **2016**, *99*, 203–213. [[CrossRef](#)]
3. Fisne, A.; Esen, O. Coal and gas outburst hazard in Zonguldak Coal Basin of Turkey, and association with geological parameters. *Nat. Hazards* **2014**, *74*, 1363–1390. [[CrossRef](#)]

4. Bulat, A.; Mineev, S.; Pursova, A. Generating methane adsorption under relaxation of molecular structure of coal. *J. Min. Sci.* **2016**, *52*, 70–77. [[CrossRef](#)]
5. Wang, Z.; Hurter, S.; You, Z.; Honari, V.; Sun, Y.; Zhang, S. Influences of negative pressure on air-leakage of coal seam gas extraction: Laboratory and CFD-DEM simulations. *J. Petrol. Sci. Eng.* **2021**, *196*, 107731. [[CrossRef](#)]
6. Wu, Y.; Wang, D.; Wei, J.; Yao, B.; Zhang, H.; Fu, J.; Zeng, F. Damage constitutive model of gas-bearing coal using industrial CT scanning technology. *J. Nat. Gas Sci. Eng.* **2022**, *101*, 104543. [[CrossRef](#)]
7. Li, Q.; Liang, Y.; Zou, Q. Seepage and Damage Evolution Characteristics of Gas-Bearing Coal under Different Cyclic Loading-Unloading Stress Paths. *Processes* **2018**, *6*, 190. [[CrossRef](#)]
8. Jiang, B.; Zhao, Y.; Lin, B.; Liu, T. Effect of faults on the pore structure of coal and its resultant change on gas emission. *J. Pet. Sci. Eng.* **2021**, *195*, 107919. [[CrossRef](#)]
9. Niu, Y.; Wang, E.; Li, Z. A study on moment tensor inversion of acoustic emission response on damaging localization of gas-bearing coal under load. *Sci. Rep.* **2022**, *12*, 16360. [[CrossRef](#)]
10. Zagorcak, R.; Thomas, H. Dynamic transport and reaction behaviour of high-pressure gases in high-rank coal. *J. Nat. Gas Sci. Eng.* **2019**, *71*, 102978. [[CrossRef](#)]
11. Du, F.; Wang, K.; Wang, G. Investigation of the acoustic emission characteristics during deformation and failure of gas-bearing coal-rock combined bodies. *J. Loss Prev. Process Ind.* **2018**, *55*, 253–266. [[CrossRef](#)]
12. Mou, J.; Liu, H.; Zou, Y.; Li, Q. A new method to determine the sensitivity of coal and gas outburst prediction index. *Arab. J. Geosci.* **2020**, *13*, 465. [[CrossRef](#)]
13. Guo, B.; Li, Y.; Jiao, F.; Luo, T.; Ma, Q. Experimental study on coal and gas outburst and the variation characteristics of gas pressure. *Geomech. Geophys. Geo Energy Gro Resour.* **2018**, *4*, 355–368. [[CrossRef](#)]
14. Xu, T.; Tang, C.; Yang, T. Numerical investigation of coal and gas outbursts in underground collieries. *Int. J. Rock Mech. Min. Sci.* **2006**, *43*, 905–919. [[CrossRef](#)]
15. Wang, Z.; Sun, Y.; Wang, Y.; Zhang, J.; Sun, Z. A coupled model of air leakage in gas drainage and an active support sealing method for improving drainage performance. *Fuel* **2019**, *237*, 1217–1227. [[CrossRef](#)]
16. Wang, Z.; Sun, Y.; Li, Z.; Wang, Y.; You, Z. Multiphysics responses of coal seam gas extraction with borehole sealed by active support sealing method and its applications. *J. Nat. Gas Sci. Eng.* **2022**, *100*, 104466. [[CrossRef](#)]
17. Qin, H.J.; Wei, J.P.; Li, D.H.; Wu, Z.Q. Research on the mechanism of in-situ stress in the process of coal and gas outburst. *J. China Univ. Min. Technol.* **2021**, *50*, 933–942.
18. Cao, J.; Zhao, X.; Liu, Y. Numerical simulation on multiphysics field distribution characteristics of coal and gas outburst. *Min. Saf. Environ. Prot.* **2021**, *48*, 7–11.
19. Feng, C.; Zhang, J.H.; Zhang, Q.L. Hematite's Dynamic Compressive Strength and Crushing Features under Impact Load. *J. Zhengzhou Univ.* **2019**, *51*, 110–115.
20. Zhang, Q.; Yue, J.; Liu, C.; Feng, C.; Li, H. Study of automated top-coal caving in extra-thick coal seams using the continuum-discontinuum element method. *Int. J. Rock Mech. Min. Sci.* **2019**, *122*, 104033. [[CrossRef](#)]
21. Zhang, Q.; Yuan, R.; Wang, S.; Li, D.; Li, H.; Zhang, X. Optimizing simulation and analysis of automated top-coal drawing technique in extra-thick coal seams. *Energies* **2020**, *13*, 232. [[CrossRef](#)]
22. Zhang, Q.; Zhi, Z.; Feng, C.; Li, R.; Yue, J.; Cong, J. Using Continuum-Discontinuum Element Method to Model the Foliation-Affected Fracturing in Rock Brazilian Test. *Adv. Civ. Eng.* **2021**, *2021*, 1–9. [[CrossRef](#)]
23. Feng, C.; Li, S.; Liu, X.; Zhang, Y. A semi-spring and semi-edge combined contact model in CDEM and its application to analysis of Jiweishan landslide. *J. Rock Mech. Geotech. Eng.* **2014**, *6*, 26–35. [[CrossRef](#)]
24. Feng, C.; Li, S.H.; Hao, W.H.; Ge, W. Numerical simulation for penetrating and blasting process of EPW based on CDEM. *J. Vib. Shock.* **2017**, *36*, 11–26.
25. Lin, Q.; Feng, C.; Zhu, X.; Zhang, G.; Li, S. Evolution characteristics of crack and energy of low-grade highway under impact load. *Int. J. Pavement Eng.* **2021**, *23*, 3182–3197. [[CrossRef](#)]
26. Zhang, Q.; Zhi, Z.; Feng, C.; Cai, Y.; Pang, G.; Yue, J. Investigation of concrete pavement cracking under multi-head impact loading via the continuum-discontinuum element method. *Int. J. Impact Eng.* **2020**, *135*, 103410. [[CrossRef](#)]
27. Xue, J.; Zhao, T. Deformation and fracture characteristics of coal gangue interbedded samples under loading and unloading conditions. *Adv. Civ. Eng.* **2022**, *2022*, 7734078. [[CrossRef](#)]
28. Wu, J.; Yan, L. Comparison study on two kinds of indirect measurement methods of tensile strength of coal in lab. *Chin. J. Rock Mech. Eng.* **2004**, *23*, 1643–1647.
29. Xie, J.; Gao, M.; Zhang, R.; Liu, J.; Lu, T.; Wang, M. Gas flow characteristics of coal samples with different levels of fracture network complexity under triaxial loading and unloading conditions. *J. Pet. Sci. Eng.* **2020**, *195*, 107606. [[CrossRef](#)]

**Disclaimer/Publisher's Note:** The statements, opinions and data contained in all publications are solely those of the individual author(s) and contributor(s) and not of MDPI and/or the editor(s). MDPI and/or the editor(s) disclaim responsibility for any injury to people or property resulting from any ideas, methods, instructions or products referred to in the content.